nature medicine

Young blood reverses age-related impairments in cognitive function and synaptic plasticity in mice

Saul A Villeda[1–6], Kristopher E Plambeck[1,2,10], Jinte Middeldorp[6,10], Joseph M Castellano[6,10], Kira I Mosher[6,7,10], Jian Luo[6], Lucas K Smith[1,2], Gregor Bieri[1,2,6,7], Karin Lin[1–3], Daniela Berdnik[6], Rafael Wabl[6], Joe Udeochu[1,2,4], Elizabeth G Wheatley[1,2,5], Bende Zou[8], Danielle A Simmons[6], Xinmin S Xie[8], Frank M Longo[6] & Tony Wyss-Coray[6,7,9]

As human lifespan increases, a greater fraction of the population is suffering from age-related cognitive impairments, making it important to elucidate a means to combat the effects of aging[1,2]. Here we report that exposure of an aged animal to young blood can counteract and reverse pre-existing effects of brain aging at the molecular, structural, functional and cognitive level. Genome-wide microarray analysis of heterochronic parabionts—in which circulatory systems of young and aged animals are connected—identified synaptic plasticity–related transcriptional changes in the hippocampus of aged mice. Dendritic spine density of mature neurons increased and synaptic plasticity improved in the hippocampus of aged heterochronic parabionts. At the cognitive level, systemic administration of young blood plasma into aged mice improved age-related cognitive impairments in both contextual fear conditioning and spatial learning and memory. Structural and cognitive enhancements elicited by exposure to young blood are mediated, in part, by activation of the cyclic AMP response element binding protein (Creb) in the aged hippocampus. Our data indicate that exposure of aged mice to young blood late in life is capable of rejuvenating synaptic plasticity and improving cognitive function.

Aging drives cognitive impairments and susceptibility to degenerative disorders in healthy individuals[3–6] by structurally and functionally changing the adult brain[3,7–13]. Considering the increase in the proportion of elderly humans[1,2], it is important to identify a means for maintaining cognitive integrity by protecting against, or even counteracting, the aging process. In aged animals, exposure to young blood through heterochronic parabiosis improves stem cell function in muscle[14,15], liver[14], spinal cord[16] and the brain[12] and ameliorates cardiac hypertrophy[17]. However, whether enhancements of young blood extend beyond regeneration in the aged brain is unknown, raising the question of whether young blood can counteract aging and rejuvenate cognitive processes.

In humans and mice, the hippocampus is particularly vulnerable to aging, exhibiting downregulation of plasticity-related genes, reduced spine density, decreased synaptic plasticity and impairments in associated cognitive functions[3–13,18–20]. We first performed genome-wide microarray analysis of hippocampi from aged (18 months) isochronic (aged-aged) and aged (18 months) heterochronic (aged-young) parabionts (**Fig. 1a**). We observed a distinct gene expression profile between the two parabiont groups (**Fig. 1c** and **Supplementary Table 1**) and identified synaptic plasticity regulation as one of the top gene ontology enrichment categories associated with heterochronic parabiosis. Furthermore, Ingenuity Pathway Analysis (IPA) detected prominent involvement of plasticity-related signaling pathways, including Creb[21], in the top-signaling network (**Fig. 1b**). Together our data reveal a transcriptional profile that is indicative of plasticity changes in heterochronic parabionts.

We then used immunohistochemistry to examine a subset of identified genes in a second cohort of parabionts (**Fig. 1d–g**). We observed increased numbers of cells expressing the immediate early genes Egr1 (**Fig. 1d,e**) and c-Fos (**Fig. 1d,f**) and a corresponding increase in phosphorylated Creb (**Fig. 1d,g**) in the dentate gyrus (DG) of heterochronic compared to isochronic parabionts. Although we observed increased phosphorylated Creb in the CA1 region, we detected no changes in immediate early genes in heterochronic parabionts (**Supplementary Fig. 1a–c**). We confirmed age-related differences in immediate early gene expression and Creb phosphorylation between young and aged unpaired animals (**Supplementary Fig. 2**). Molecular changes were not elicited by the parabiosis procedure (**Supplementary Fig. 1d–i**), and we observed no differences in general health, maintenance behavior or stress responses between

[1]Department of Anatomy, University of California San Francisco, San Francisco, California, USA. [2]The Eli and Edythe Broad Center for Regeneration Medicine and Stem Cell Research, San Francisco, California, USA. [3]Neuroscience Graduate Program, University of California San Francisco, San Francisco, California, USA. [4]Biomedical Sciences Graduate Program, University of California San Francisco, San Francisco, California, USA. [5]Developmental and Stem Cell Biology Graduate Program, University of California San Francisco, San Francisco, California, USA. [6]Department of Neurology and Neurological Sciences, Stanford University School of Medicine, Stanford, California, USA. [7]Neuroscience Graduate Program, Stanford University School of Medicine, Stanford, California, USA. [8]AfaSci Research Laboratory, Redwood City, California, USA. [9]Center for Tissue Regeneration, Repair and Restoration, VA Palo Alto Health Care System, Palo Alto, California, USA. [10]These authors contributed equally to this work. Correspondence should be addressed to S.A.V. (saul.villeda@ucsf.edu) or T.W.-C. (twc@stanford.edu).

Received 8 February; accepted 16 April; published online 4 May 2014; doi:10.1038/nm.3569

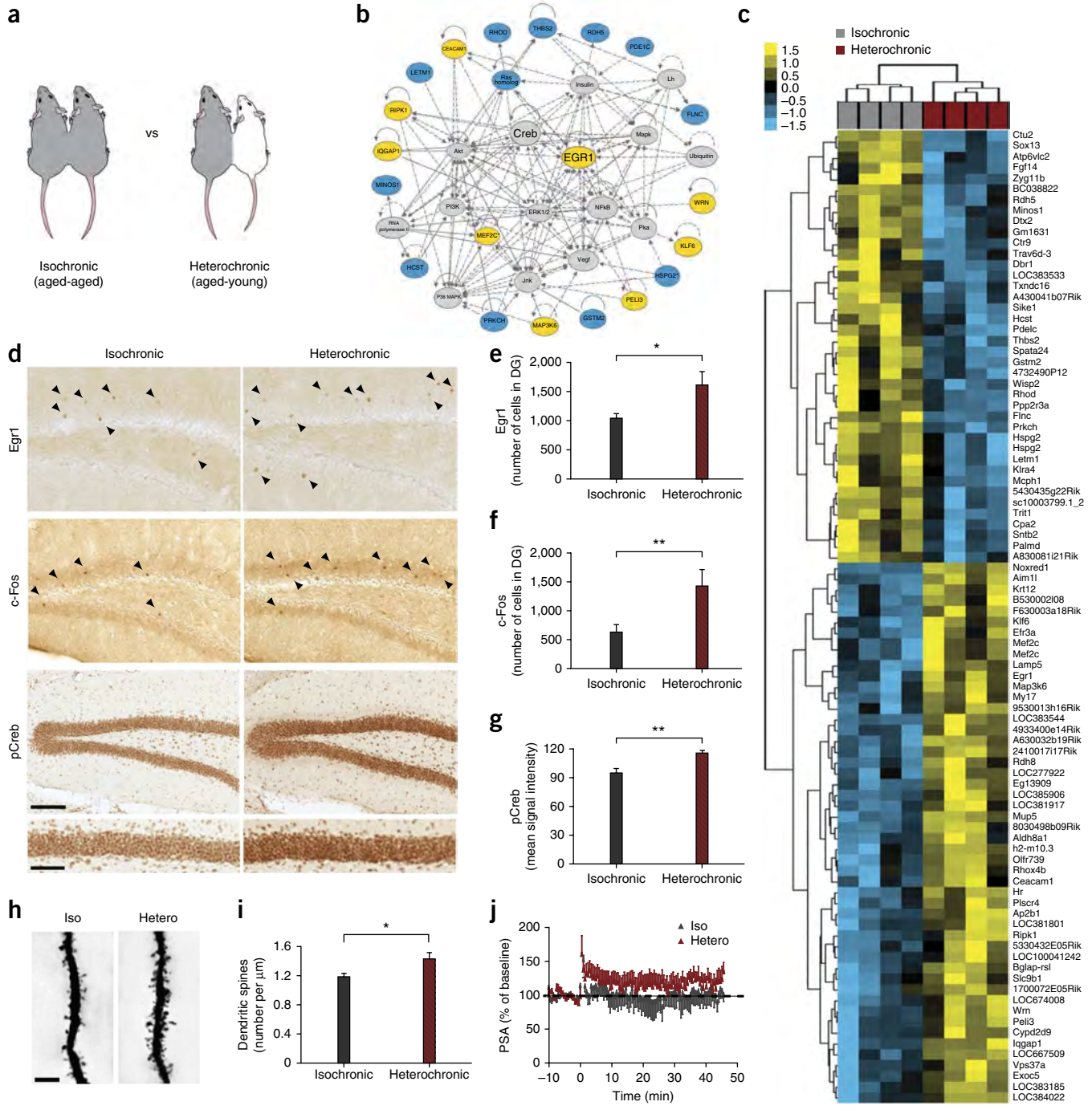

Figure 1 Heterochronic parabiosis enhances dendritic spine number and synaptic plasticity in the aged hippocampus and elicits a plasticity-related expression profile. (**a**) Schematic depicting the parabiotic pairings. (**b**,**c**) Microarray analysis performed on the hippocampi of aged (18 months) isochronic and heterochronic parabionts 5 weeks after surgery. $n = 4$ mice per group. For all analyses, downregulated genes are shown in shades of blue, and upregulated genes are shown in shades of yellow. (**b**) Biological pathways involved in synaptic plasticity identified as part of the top signaling network ($P < 0.05$) using IPA software based on differentially expressed genes in isochronic and heterochronic parabionts. Inferred molecular interactions identified by IPA are shown in gray. (**c**) Heat map generated by unsupervised hierarchical clustering with a data set of genes differentially expressed between hippocampi of aged isochronic (Iso) and heterochronic (Hetero) parabionts using a cutoff at $P < 0.01$ and d score > 2 on the basis of Significance Analysis of Microarray (SAM). Color bars reflect the z scores. (**d**–**j**) Histological and electrophysiological analysis performed on aged (18 months) isochronic ($n = 6$) and heterochronic ($n = 5$) parabionts analyzed 5 weeks after surgery. (**d**) Immunohistochemical detection of Egr1, c-Fos and phosphorylated Creb (pCreb) protein in the DG of the hippocampi of aged isochronic and heterochronic parabionts. Arrowheads indicate individual cells. Scale bars, 100 µm (low magnification); 50 µm (high magnification). (**e**–**g**) Quantification of the immunostaining for Egr1 (**e**), c-Fos (**f**) and pCreb (**g**). Five sections per mouse were analyzed. (**h**,**i**) Representative Golgi stain image (**h**; scale bar, 5 µm) and quantification of dendritic spine density on tertiary branches (**i**). Five neurons per mouse were analyzed. (**j**) Population spike amplitude (PSA) recorded from the DG of aged parabionts. Representative LTP levels are shown for isochronic and heterochronic parabionts. All data are shown as the mean ± s.e.m. $^*P < 0.05$, $^{**}P < 0.01$, t test (**e**–**g**,**i**).

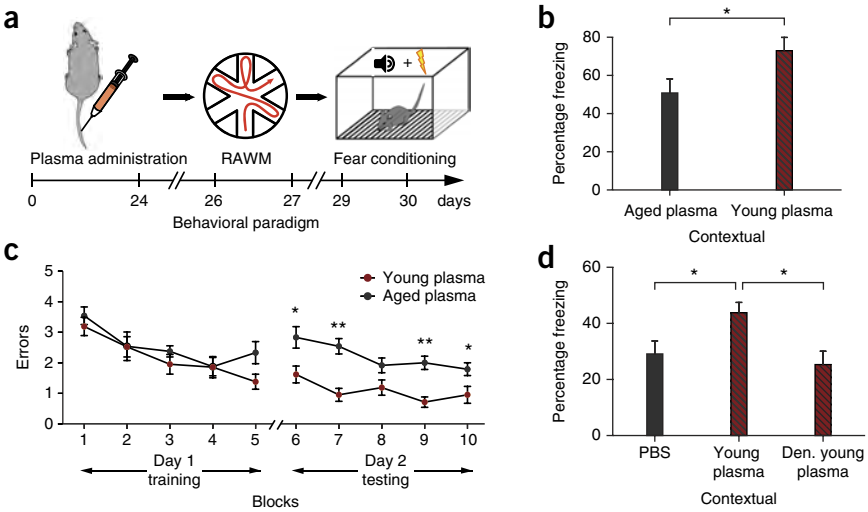

Figure 2 Administration of young blood plasma improves hippocampal-dependent learning and memory in aged mice. (**a**–**c**) Results from aged (18 months) mice that were cognitively tested after systemic treatment with young (3 months) or aged (18 months) plasma eight times over 24 d (100 µl per intravenous injection). $n = 8$ mice per group. (**a**) Schematic illustrating the chronological order used for plasma treatment and cognitive testing. (**b**,**c**) Hippocampal-dependent learning and memory assessed by contextual fear conditioning (**b**) and RAWM (**c**) after plasma treatment. (**b**) Percentage freezing time 24 h after training. (**c**) Number of entry-arm errors before finding the platform. (**d**) Cognitive testing by contextual fear conditioning in aged mice after systemic treatment with saline ($n = 11$), young plasma ($n = 12$) or heat-denatured (den.) young plasma ($n = 10$) (100 µl per intravenous injection). Results are shown as the percentage freezing time 24 h after training. All data are shown as the mean ± s.e.m. $^*P < 0.05$, $^{**}P < 0.01$, *t* test (**b**), repeated measures analysis of variance (ANOVA) with Bonferroni *post-hoc* test (**c**) or ANOVA with Tukey's *post-hoc* test (**d**).

isochronic and heterochronic parabionts (**Supplementary Fig. 3**). These data suggest that synaptic plasticity in the aged hippocampus may be enhanced by exposure to young blood.

Next we characterized structural changes in the hippocampus that underlie synaptic plasticity in a third cohort of parabionts by Golgi analysis. Dendritic spine number on granule cell neurons in the DG (**Fig. 1h**,**i**), but not the CA1 (**Supplementary Fig. 4a**), increased in heterochronic parabionts. We found no differences in dendritic complexity between the groups of parabionts (**Supplementary Fig. 4b**–**d**). These structural data indicate that exposure to young blood increases spine number in the aged DG.

To investigate functional changes, we performed extracellular electrophysiological recordings on hippocampal slices from a fourth cohort of parabionts (**Fig. 1j**). Although long-term potentiation (LTP) in the DG of isochronic parabionts quickly reached baseline levels, LTP in heterochronic parabionts was maintained above baseline throughout the recording period (**Fig. 1j**). We detected no changes in synaptic strength (**Supplementary Fig. 4e**). These functional data indicate that synaptic plasticity in aged mice is enhanced by exposure to young blood.

Given that LTP is a putative functional correlate of learning and memory[22,23], we postulated that exposure to young blood could enhance cognitive processes. First we used contextual fear conditioning and radial arm water maze (RAWM) paradigms to confirm age-related impairments in hippocampal-dependent learning and memory (**Supplementary Fig. 5**). Subsequently, in an independent cohort of aged mice, we intravenously injected 100 µl of young (3 months) or aged (18 months) plasma eight times over 3 weeks before cognitive testing (**Fig. 2a**). During fear conditioning training, all mice exhibited similar baseline freezing (**Supplementary Fig. 6a**). However, mice receiving young plasma demonstrated increased freezing in contextual (**Fig. 2b**), but not cued (**Supplementary Fig. 6b**), memory testing. In the RAWM, aged mice, regardless of plasma treatment, showed similar spatial learning for the visible platform (**Fig. 2c**) and swim speeds (**Supplementary Fig. 6c**) during the training phase. However, aged mice given young plasma demonstrated enhanced learning and memory for hidden platform location during the testing phase (**Fig. 2c**). We detected no differences between untreated aged mice and aged mice treated with aged plasma (**Supplementary Fig. 7**). Additionally, we corroborated our findings in an additional, independent fear-conditioning experiment in which we systemically administered saline, young plasma or heat-denatured young plasma to aged animals (**Fig. 2d** and **Supplementary Fig. 8**). Although we observed increased freezing during contextual memory testing in the animals treated with young plasma, the beneficial effects of young plasma were mitigated by heat denaturation (**Fig. 2d**). Together these behavioral data indicate that administration of soluble heat-labile factors from young blood rejuvenates cognitive function in aged animals.

To gain mechanistic insight, we expanded on the transcriptional analysis (**Fig. 1b**) and examined whether abrogation of Creb signaling within the hippocampus of aged animals could mitigate the structural and cognitive enhancements elicited by young blood (**Fig. 3**). We generated adeno-associated viruses (AAVs) overexpressing a dominant-negative DNA binding–incompetent form of Creb (K-Creb) that inhibits endogenous Creb signaling[24] in tandem with a GFP reporter (**Supplementary Fig. 9a**,**b**). We confirmed K-Creb expression (**Supplementary Fig. 9c**,**d**) and transcriptional inhibition of Creb (**Supplementary Fig. 9e**) *in vitro*. AAVs encoding K-Creb or GFP were stereotaxically injected into contralateral hippocampi of adult mice. Overexpression of K-Creb was confirmed *in vivo* (**Fig. 3a**–**c**).

Dendritic spine density was assessed by AAV-mediated neuronal tracing after overexpression of K-Creb in a fifth cohort of parabionts (**Fig. 3d**). We stereotaxically injected aged unpaired animals with low-titer (5×10^8 viral particles per ml) AAVs encoding K-Creb or GFP into the contralateral DG to visualize dendritic spines by GFP expression (**Fig. 3e**). After recovery for 2 weeks, we connected the animals by isochronic or heterochronic parabiosis. Consistent with the Golgi analysis, dendritic spine density increased in granule cell neurons overexpressing GFP in heterochronic compared to isochronic parabionts (**Fig. 3f**). These changes in dendritic spine density were abrogated in neurons overexpressing K-Creb (**Fig. 3f**). To corroborate the structural results, we assessed dendritic spine density in a sixth cohort of parabionts using a lentivirus-mediated RNA interference approach that silences endogenous Creb by shRNAs (**Supplementary Figs. 10** and **11**). We confirmed abrogation of Creb expression in an N2A neuronal cell line (**Supplementary Fig. 10**) and in the hippocampi of adult mice after stereotaxic injection

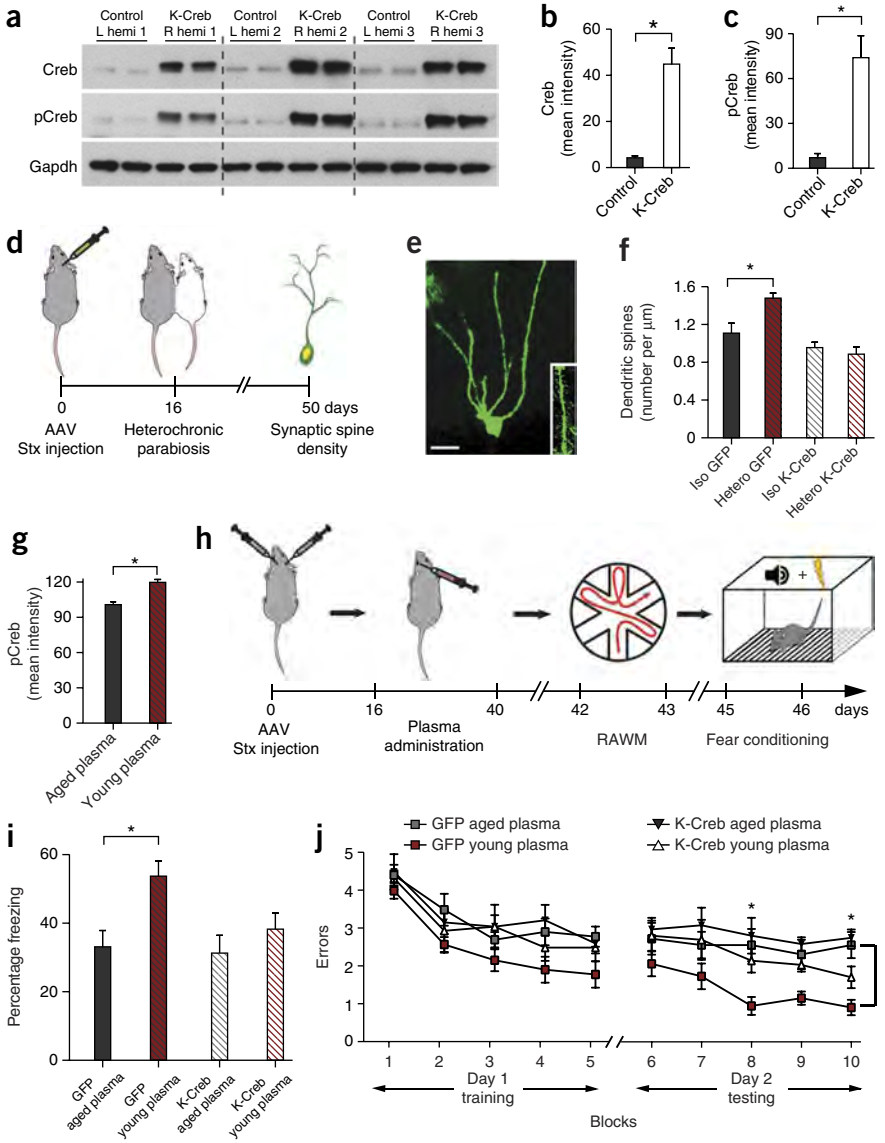

Figure 3 Creb mediates the enhancements in dendritic spine number and hippocampal-dependent learning and memory elicited by young blood in aged mice. (**a**–**c**) Western blot analysis (**a**) and quantification by optical intensity (**b**,**c**) of Creb overexpression and pCreb in isolated hippocampi of adult mice that were contralaterally locally infected with AAVs encoding either K-Creb or GFP. Hemi, hemisphere. (**d**) Schematic illustrating the chronological order used for AAV delivery of K-Creb or GFP and the parabiosis procedure. (**e**,**f**) Representative confocal image of an AAV-infected GFP-positive neuron and dendritic spines (scale bar, 25 µm; **e**) and quantification of spine density on tertiary branches (**f**). Five to seven neurons per mouse were analyzed. $n = 8$ isochronic and 6 heterochronic parabionts. (**g**) Quantification of immunostaining for pCreb in the DG of the hippocampi of aged animals systemically administered with young (3 months) or aged (18 months) plasma. $n = 5$ mice per group, and five sections per mouse were analyzed. (**h**–**j**) Cognitive testing of aged mice that were given bilateral stereotaxic injections of AAV encoding K-Creb ($n = 8$ per group) or GFP ($n = 10$ per group) into the DG followed by systemic treatment with young or aged plasma eight times over 24 d (100 µl per intraorbital injection). (**h**) Schematic illustrating the chronological order used for AAV delivery, plasma treatment and cognitive testing. Stx, stereotaxic. (**i**,**j**) Hippocampal-dependent learning and memory assessed by contextual fear conditioning (**i**) and RAWM (**j**) after plasma treatment. (**i**) Percentage freezing time 24 h after training. (**j**) Number of entry-arm errors before finding platform. All data are shown as the mean ± s.e.m. $^*P < 0.05$, *t* test (**b**,**c**,**g**), ANOVA with Dunnett's *post-hoc* test (**i**) or repeated measures ANOVA with Bonferroni *post-hoc* test (**j**).

(**Supplementary Fig. 11a**,**b**). Consistent with previous data, the enhancements in dendritic spine density observed in aged heterochronic parabionts were mitigated after silencing of Creb expression (**Supplementary Fig. 11c**,**d**). Together these data indicate that Creb signaling is necessary for increased spine number in aged heterochronic parabionts.

Next we examined phosphorylated Creb in the DG of aged animals systemically treated with plasma from young or aged mice by immunohistochemistry. Creb phosphorylation increased in the DG after administration of young plasma (**Fig. 3g**). We then stereotaxically injected a third cohort of aged animals with a high-titer (1.2×10^9 viral particles per ml) of AAVs encoding K-Creb or GFP bilaterally in the DG (**Fig. 3h** and **Supplementary Fig. 12a**). After recovery for 2 weeks, we intraorbitally injected 100 µl of young or aged plasma eight times over 3 weeks before cognitive testing (**Fig. 3h**). All groups showed similar baseline freezing values during fear conditioning training (**Supplementary Fig. 12c**). Consistent with previous data, we observed increased freezing during contextual (**Fig. 3i**), but not cued (**Supplementary Fig. 12d**), memory testing in animals overexpressing GFP and treated with young plasma compared to those treated with aged plasma. Notably, the effects of young plasma on contextual fear conditioning were mitigated in animals overexpressing K-Creb (**Fig. 3i**). In the RAWM, all groups showed similar spatial learning capacity (**Fig. 3j**) and swim speeds (**Supplementary Fig. 12b**) during the training phase. However, learning and memory for platform location were improved in animals overexpressing GFP and treated with young plasma compared to those treated with aged plasma (**Fig. 3j**). Although not completely mitigated, enhancements in spatial learning and memory were reduced in animals overexpressing K-Creb (**Fig. 3j**). We detected no differences in learning or memory between aged animals overexpressing GFP or K-Creb and treated with aged plasma (**Fig. 3i**,**j**). These behavioral data indicate that cognitive improvements observed in aged animals after systemic administration with young plasma are mediated in part by Creb.

Taken together, our data demonstrate that exposure to young blood counteracts aging at the molecular, structural, functional and cognitive levels in the aged hippocampus. Mechanistically, we identified Creb as one member of the regulatory network underlying structural and cognitive enhancements by young blood. We previously observed increased neurogenesis in the DG of aged heterochronic parabionts[12], and although we do not exclude a role for neurogenesis in the current study, data remain inconsistent regarding a causal link between

decreased neurogenesis and age-related cognitive decline[25–27]. This suggests that cognitive improvements elicited by young blood may not be limited to neurogenesis but may also be due to enhancements in synaptic plasticity. Additionally, we previously identified 'pro-aging' factors in young heterochronic parabionts as negative regulators of neurogenesis and cognition; however, these factors were unchanged in aged heterochronic parabionts[12]. Correspondingly, our studies suggest two distinct strategies for reversing aging phenotypes. One possibility is that introducing 'pro-youthful' factors from young blood can reverse age-related impairments in the brain, and a second possibility is that abrogating pro-aging factors from aged blood can counteract such impairments. These two possibilities are not mutually exclusive, warrant further investigation and may each provide a successful strategy to combat the effects of aging. It is important to consider that the results of this study are currently limited to aged mice; however, future studies are warranted in aged humans and potentially those suffering from age-related neurodegenerative disorders.

METHODS

Methods and any associated references are available in the online version of the paper.

Note: Any Supplementary Information and Source Data files are available in the online version of the paper.

ACKNOWLEDGMENTS

We thank A. Eggel, K. Lucin and N. Woodling for critical review and advice, and D. Jing and F. Lee (Cornell University) for Golgi stain reagents. This work was funded by California Institute for Regenerative Medicine (CIRM) fellowships (K.E.P. and K.L.), a Netherlands Organization for Scientific Research (NWO) Rubicon fellowship (J.M.), a Child Health Research Institute fellowship (Stanford National Institutes of Health (NIH)/National Center for Research Resources CTSA-UL1-RR025744, J.M.C.), a Jane Coffin Childs fellowship (J.M.C.), National Science Foundation fellowships (K.I.M. and J.U.), a National Research Service Award fellowship (1F31-AG034045-01, S.A.V.), anonymous (T.W.-C.), Veterans Affairs (T.W.-C.), the National Institute on Aging (AG045034, AG03144, T.W.-C.), CIRM (T.W.-C.), the University of California San Francisco (UCSF) Program for Breakthrough Biomedical Research, the Sandler Foundation (S.A.V.), the UCSF Clinical and Translational Science Institute (UL1-TR000004, S.A.V.) and an NIH Director's Independence Award (DP5-OD12178, S.A.V.).

AUTHOR CONTRIBUTIONS

S.A.V., K.E.P., J.M., J.M.C., K.I.M., J.L., L.K.S. and K.L. performed parabiosis. S.A.V., K.I.M., G.B. and D.B. performed and/or analyzed microarray. S.A.V., K.E.P., R.W. and E.G.W. performed histological studies. J.M. and D.A.S. performed Golgi studies. B.Z. and X.S.X. performed electrophysiological studies. S.A.V., K.E.P., J.M.C., J.L., L.K.S., G.B., K.L. and J.U. performed plasma cognitive studies. J.M.C. performed maintenance and stress studies. J.M.C. and S.A.V. performed the denaturation study. K.E.P. and G.B. generated viral constructs. K.E.P. performed viral studies. F.M.L. provided reagents. S.A.V. and T.W.-C. designed and supervised the study and wrote the manuscript.

COMPETING FINANCIAL INTERESTS

The authors declare competing financial interests: details are available in the online version of the paper.

1. Hebert, L.E., Scherr, P.A., Bienias, J.L., Bennett, D.A. & Evans, D.A. Alzheimer disease in the US population: prevalence estimates using the 2000 census. *Arch. Neurol.* **60**, 1119–1122 (2003).
2. Bishop, N.A., Lu, T. & Yankner, B.A. Neural mechanisms of ageing and cognitive decline. *Nature* **464**, 529–535 (2010).
3. Hedden, T. & Gabrieli, J.D. Insights into the ageing mind: a view from cognitive neuroscience. *Nat. Rev. Neurosci.* **5**, 87–96 (2004).
4. Raz, N., Gunning-Dixon, F.M., Head, D., Dupuis, J.H. & Acker, J.D. Neuroanatomical correlates of cognitive aging: evidence from structural magnetic resonance imaging. *Neuropsychology* **12**, 95–114 (1998).
5. Mattson, M.P. & Magnus, T. Ageing and neuronal vulnerability. *Nat. Rev. Neurosci.* **7**, 278–294 (2006).
6. Rapp, P.R. & Heindel, W.C. Memory systems in normal and pathological aging. *Curr. Opin. Neurol.* **7**, 294–298 (1994).
7. Andrews-Hanna, J.R. *et al.* Disruption of large-scale brain systems in advanced aging. *Neuron* **56**, 924–935 (2007).
8. Scheff, S.W., Price, D.A., Schmitt, F.A., DeKosky, S.T. & Mufson, E.J. Synaptic alterations in CA1 in mild Alzheimer disease and mild cognitive impairment. *Neurology* **68**, 1501–1508 (2007).
9. Nicholson, D.A., Yoshida, R., Berry, R.W., Gallagher, M. & Geinisman, Y. Reduction in size of perforated postsynaptic densities in hippocampal axospinous synapses and age-related spatial learning impairments. *J. Neurosci.* **24**, 7648–7653 (2004).
10. Smith, T.D., Adams, M.M., Gallagher, M., Morrison, J.H. & Rapp, P.R. Circuit-specific alterations in hippocampal synaptophysin immunoreactivity predict spatial learning impairment in aged rats. *J. Neurosci.* **20**, 6587–6593 (2000).
11. Morrison, J.H. & Baxter, M.G. The ageing cortical synapse: hallmarks and implications for cognitive decline. *Nat. Rev. Neurosci.* **13**, 240–250 (2012).
12. Villeda, S.A. *et al.* The ageing systemic milieu negatively regulates neurogenesis and cognitive function. *Nature* **477**, 90–94 (2011).
13. Pavlopoulos, E. *et al.* Molecular mechanism for age-related memory loss: the histone-binding protein RbAp48. *Sci. Transl. Med.* **5**, 200ra115 (2013).
14. Conboy, I.M. *et al.* Rejuvenation of aged progenitor cells by exposure to a young systemic environment. *Nature* **433**, 760–764 (2005).
15. Brack, A.S. *et al.* Increased Wnt signaling during aging alters muscle stem cell fate and increases fibrosis. *Science* **317**, 807–810 (2007).
16. Ruckh, J.M. *et al.* Rejuvenation of regeneration in the aging central nervous system. *Cell Stem Cell* **10**, 96–103 (2012).
17. Loffredo, F.S. *et al.* Growth differentiation factor 11 is a circulating factor that reverses age-related cardiac hypertrophy. *Cell* **153**, 828–839 (2013).
18. Geinisman, Y., de Toledo-Morrell, L. & Morrell, F. Loss of perforated synapses in the dentate gyrus: morphological substrate of memory deficit in aged rats. *Proc. Natl. Acad. Sci. USA* **83**, 3027–3031 (1986).
19. Rosenzweig, E.S. & Barnes, C.A. Impact of aging on hippocampal function: plasticity, network dynamics, and cognition. *Prog. Neurobiol.* **69**, 143–179 (2003).
20. Small, S.A., Schobel, S.A., Buxton, R.B., Witter, M.P. & Barnes, C.A. A pathophysiological framework of hippocampal dysfunction in ageing and disease. *Nat. Rev. Neurosci.* **12**, 585–601 (2011).
21. Alberini, C.M. Transcription factors in long-term memory and synaptic plasticity. *Physiol. Rev.* **89**, 121–145 (2009).
22. Bliss, T.V. & Collingridge, G.L. A synaptic model of memory: long-term potentiation in the hippocampus. *Nature* **361**, 31–39 (1993).
23. Frey, U. & Morris, R.G. Synaptic tagging and long-term potentiation. *Nature* **385**, 533–536 (1997).
24. Jeong, H. *et al.* Sirt1 mediates neuroprotection from mutant huntingtin by activation of the TORC1 and CREB transcriptional pathway. *Nat. Med.* **18**, 159–165 (2012).
25. Merrill, D.A., Karim, R., Darraq, M., Chiba, A.A. & Tuszynski, M.H. Hippocampal cell genesis does not correlate with spatial learning ability in aged rats. *J. Comp. Neurol.* **459**, 201–207 (2003).
26. Bizon, J.L. & Gallagher, M. Production of new cells in the rat dentate gyrus over the lifespan: relation to cognitive decline. *Eur. J. Neurosci.* **18**, 215–219 (2003).
27. Drapeau, E. *et al.* Spatial memory performances of aged rats in the water maze predict levels of hippocampal neurogenesis. *Proc. Natl. Acad. Sci. USA* **100**, 14385–14390 (2003).

ONLINE METHODS

Institutions. Every effort was put forth into ensuring that multiple investigators were able to reproduce the basic findings at both the University of California San Francisco (UCSF) and Stanford/VA Palo Alto using different facilities, instruments and tools. For behavioral experiments, efforts were made to equate testing protocols between institutions, but a number of environmental factors differing between institutions persisted. Such confounding factors could directly result in the differences observed between the two institutions in animal baseline freezing and errors committed. In particular, the investigators, animal husbandry methods, type of animal chow provided, vivarium noise levels and overall behavior room dimensions and layouts differed between the institutions. Additionally, plasma denaturation and K-Creb cognitive experiments were conducted over 2 years after the first plasma–treatment cognitive experiments.

Animal models. The following mouse lines were used: C57BL/6 young mice (The Jackson Laboratory) and C57BL/6 young and aged mice (National Institutes of Aging). All studies were done in male mice. The numbers of mice used to result in statistically significant differences were calculated using standard power calculations with $\alpha = 0.05$ and a power of 0.8. We used an online tool (http://www.stat.uiowa.edu/~rlenth/Power/index.html) to calculate power and sample sizes based on experience with the respective tests, the variability of the assays and inter-individual differences within groups. Mice were housed under specific pathogen-free conditions under a 12 h light, 12 h dark cycle, and all animal handling and use was in accordance with institutional guidelines approved by the UCSF Institutional Animal Care and Use Committee and the VA Palo Alto Committee on Animal Research.

Parabiosis. Parabiosis surgery followed previously described procedures[12,14]. Mirror-image incisions at the left and right flanks were made through the skin, and shorter incisions were made through the abdominal wall. The peritoneal openings of the adjacent parabionts were sutured together. Elbow and knee joints from each parabiont were sutured together, and the skin of each mouse was stapled (9-mm Autoclip, Clay Adams) to the skin of the adjacent parabiont. Each mouse was injected subcutaneously with enrofloxacin (Bayer) antibiotic and buprenorphine (Butler Schein) as directed for pain and monitored during recovery. For overall health and maintenance behavior, several recovery characteristics were analyzed at various times after surgery, including paired weights, grooming and stress responses. General appearance was recorded at the indicated intervals using a basic grooming appearance scale that ranged from an absence of grooming behavior (0) to normal, healthy grooming behavior (4). Intermediate scores reflect the degree and frequency at which fur was groomed and/or maintained on various regions of the paired body, including muzzle, eyes, head, torso and legs, adapted from guidelines from Smolinsky *et al.*, 2009 (refs. 28,29).

Stereotaxic injections. Animals were placed in a stereotaxic frame and anesthetized with 2% isoflurane (Patterson Veterinary) (2 l per min oxygen flow rate) delivered through an anesthesia nose cone. Ophthalmic eye ointment was applied to the cornea to prevent desiccation during surgery. The area around the incision was trimmed. Viral solutions were injected bilaterally into the dorsal hippocampi using the following coordinates: (from bregma) anterior = −2 mm, lateral = 1.5 mm and (from skull surface) height = −2.1 mm. A 2 µl volume was injected stereotaxically over 10 min (injection speed: 0.20 µl per min) using a 5-µl 26s-gauge Hamilton syringe. To limit reflux along the injection track, the needle was maintained *in situ* for 8 min, slowly pulled out half-way and kept in position for an additional 2 min. The skin was closed using silk suture. Each mouse was injected subcutaneously with the analgesic buprenorphine (Butler Schein). Mice were single housed and monitored during recovery.

Gene microarray analysis. Hippocampi from isochronic and heterochronic parabionts were dissected, and total RNA was extracted using TRIzol reagent (Invitrogen). cDNA and cRNA were sequentially synthesized and amplified using an RNA Amplification Kit (Ambion) according to the manufacturer's protocol. cRNA was then hybridized to the Illumina beadchip array MouseWG-6 v2.0 (Illumina) according to the manufacturer's instructions. Data were analyzed by Illumina beadstudio data analysis software (Illumina) following the manufacturer's guidelines. Cluster 3.0 software was used for unsupervised hierarchical clustering of *z*-scored data sets. Java TreeView software was used for generating heat maps. A cutoff at $P < 0.01$ and absolute d score > 2 or d score > 1.5 was used based on SAM software (SAM 3.00 algorithm, http://statweb.stanford.edu/~tibs/SAM/ was applied for the data set analysis). Significantly changed probe sets were analyzed for statistically enriched pathways using IPA (Ingenuity Systems, http://www.ingenuity.com) and categorized for biological function using AmiGO (The Gene Ontology Consortium, http://www.godatabase.org/cgi-bin/amigo/go/cgi).

Immunohistochemistry. Tissue processing and immunohistochemistry were performed on free-floating sections following standard published techniques[30]. Mice were anesthetized with chloral hydrate (Sigma-Aldrich) and transcardially perfused with 0.9% saline, and brains were removed and fixed in phosphate-buffered 4% paraformaldehyde for 48 h before cryprotection with 30% sucrose. Free-floating coronal sections (40 µm) were incubated overnight with rabbit anti-Egr1 (1:500, 588, Santa Cruz), rabbit anti–c-Fos (1:500, 4-17, Millipore) or rabbit anti-pCreb (1:1,000, Ser133, 06-519, Millipore) primary antibodies, and staining was revealed using biotinylated secondary antibodies and the ABC kit (Vector) with diaminobenzidine (DAB; Sigma-Aldrich). Individual cell numbers were quantified by Egr1 and c-Fos, and pCreb was quantified as the mean signal intensity using NIH ImageJ software.

Golgi staining. After brain removal, hemispheres were immersed in 10 ml modified Golgi-Cox staining solution (courtesy of D. Jing and F. Lee at Cornell University) for 7–10 d at room temperature in the dark. Brains were transferred to 30% sucrose in dH_2O at 4 °C for 72 h. Sections (150 µm) were mounted onto slides coated with 0.3% gelatin in dH_2O. After briefly drying, slides were dipped in 40% sucrose three times and air dried for 72 h in the dark. Slides were immersed into dH_2O three times for 10 min with gentle shaking and then transferred to a developing solution for 6 min. Slides were then rinsed three times for 10 min in dH_2O, dehydrated through graded ethanol, immersed in Histoclear and then coverslipped using DPX mounting medium (Sigma-Aldrich). Neurons were traced at 100×, and all subsequent analyses were done using Neurolucida Software (v10, MBF Bioscience). Sholl analysis was performed for each neuron by placing concentric spheres at 10-µm intervals from the soma. The number of times the dendrite intersected each sphere and the total dendritic length within each sphere were quantified. Dendritic length was summed across distance in the *x*, *y*, and *z* planes and across multiple dendritic branches of the neurons that are contained within each radius.

Extracellular electrophysiology. Extracellular electrophysiology was performed as previously described[31]. Acute hippocampal slices (400-µm thick) were prepared from aged parabionts. Slices were maintained in artificial cerebrospinal fluid (ACSF; (in mM) NaCl, 124.0; KCl, 2.5; KH_2PO4, 1.2; $CaCl_2$, 2.4; $MgSO_4$, 1.3; $NaHCO_3$, 26.0; and glucose, 10.0) continuously oxygenated with 5% CO_2 and 95% O_2. Recordings were performed with an Axopatch-2B amplifier and pClamp 10.2 software (Axon Instruments). Submerged slices were continuously perfused with oxygenated ACSF at a flow rate of 2 ml per min from a reservoir by gravity feeding. Field potential (population spikes) was recorded using glass microelectrodes filled with ACSF (resistance: 4–8 MΩ). Biphasic current pulses (0.2-ms duration for one phase, 0.4 ms in total) were delivered in 10-s intervals through a concentric bipolar stimulating electrode (FHC, Inc.). No obvious synaptic depression or facilitation was observed with this frequency stimulation. To record field population spikes in the dentate gyrus, the recording electrode was placed in the lateral or medial side of the dorsal part of the dentate gyrus. The stimulating electrode was placed directly above the hippocampal fissure to stimulate the perforant pathway fibers. Signals were filtered at 1 kHz and digitized at 10 kHz. Tetanic stimulation consisted of two trains of 100 pulses (0.4-ms pulse duration, 100 Hz) delivered with an intertrain interval of 5 s. The amplitude of each population spike was measured from the initial phase of the negative wave. Up to five

doi:10.1038/nm.3569

consecutive traces were averaged for each measurement. Synaptic transmission was assessed by generating input-output curves, with the stimulus strength adjusted to be ~30% of the maximum. LTP was calculated as the mean percentage change in the amplitude of the population spike after high-frequency stimulation relative to its basal amplitude.

Western blot analysis. Mouse hippocampi were dissected after perfusion of the animal, snap frozen and lysed in RIPA lysis buffer (500 mM Tris, pH 7.4, 150 mM NaCl, 0.5% Na deoxycholate, 1% NP40, 0.1% SDS and cOmplete protease inhibitors; Roche). Tissue lysates were mixed with 4× NuPage LDS loading buffer (Invitrogen), loaded on a 4–12% SDS polyacrylamide gradient gel (Invitrogen) and subsequently transferred onto a nitrocellulose membrane. The blots were blocked in 5% milk in Tris-buffered saline with Tween (TBST) and incubated with rabbit anti-actin (1:5,000, A-5060, Sigma), mouse anti-Gapdh (1:10,000, 6C5, Abcam) rabbit anti-Creb (1:1,000, 48H2, Cell Signaling) and rabbit anti-pCreb (1:1,000, Ser133, D1G6, Cell Signaling). Horseradish peroxidase–conjugated secondary antibodies and an ECL kit (GE Healthcare/Amersham Pharmacia Biotech) were used to detect protein signals. Multiple exposures were taken to select images within the dynamic range of the film (GE Healthcare Amersham Hyperfilm ECL). Selected films were scanned (300 dots per inch) and quantified using ImageJ software (Version 1.46k). Actin bands were used for normalization.

Viral plasmids. We generated AAVs (AAV-DJ[32]) that overexpressed a DNA binding–incompetent form of Creb (K-Creb), which have been previously shown to exhibit dominant-negative inhibition of endogenous Creb signaling (Clontech)[24]. The AAV plasmids expressed a K-Creb–T2A-GFP construct under a cytomegalovirus (CMV) promoter. The K-Creb sequence was isolated using the Phusion Hot Start II DNA Polymerase (Fisher Scientific, Inc) using the following PCR primers: 5′-ATATATGCTAGCGCCACCATGACCATG GAATCTGGAGC-3′ and 5′-ATATATGGATCCATCTGATTTGTGGCAGT AAAGGTC-3′. K-Creb was then cloned into the AAV backbone using the restriction enzymes NheI and BamHI. The K-Creb construct is in frame with both the T2A domain and GFP. We generated lentiviruses (LVs) encoding shRNAs targeting endogenous Creb using a lentiviral shRNA expression system (pGreenPuro shRNA, System Biosciences) according to the manufacturer's instructions. The Creb-targeted sequences were cloned into the pGreenPuro vector (Creb, 5′-GTACAGCTGGCTAACAATGG-3′). Plasmid quality was tested with western blot analysis and sequencing. AAVs and LVs were stereotaxically injected into one hippocampus, and a control virus, based on the same viral plasmid, was injected as an internal control at the same location into the contralateral hemisphere.

Viruses. LV vectors were generated at the UCSF Viracore, and AAV vectors were generated at the Stanford Neuroscience Gene Vector and Virus Core. We used AAV-DJ[32] to efficiently infect neurons over a wide area of the hippocampus[33]. Viral titers were between 5×10^8 and 1.2×10^9 viral particles per ml.

Cell culture experiments. An N2A neuronal cell line (American Type Culture Collection, CCL-131) was used for *in vitro* experiments. Cells were plated at a confluency of 85–90% for transfection experiments. Lipofectamine 2000 (Invitrogen) was used as the transfection reagent. The culture medium (DMEM + 10% FBS) was exchanged after 6 h to reduce toxicity caused by the transfection reagent. Gene expression was assessed with the help of GFP reporters and fluorescence microscopy. Cells were lysed 24 h after transfection. Experiments were performed in triplicates. For transcriptional activity analysis of Creb, luciferase reporter plasmids (Signosis) were co-transfected with either Creb or K-Creb plasmids into N2A cells. The Luciferase reporter assay was used following the manufacturer's instructions (Promega).

Contextual fear conditioning. Our paradigm followed previously published techniques[34]. Mice learned to associate the environmental context (fear-conditioning chamber) with an aversive stimulus (mild foot shock; unconditioned stimulus, US), which enabled testing for hippocampal-dependent contextual fear conditioning. The mild foot shock was paired with a light and tone cue (conditioned stimulus, CS) in order to also assess amygdala-dependent cued fear conditioning. Conditioned fear was displayed as freezing behavior. Specific training parameters were as follows: tone duration, 30 s; level, 70 dB, 2 kHz; shock duration, 2 s; intensity, 0.6 mA. On day 1, each mouse was placed in a fear-conditioning chamber and allowed to explore for 2 min before delivery of a 30-s tone (70 dB) ending with a 2-s foot shock (0.6 mA). Two minutes later, a second CS-US pair was delivered. On day 2, each mouse was first placed in the fear-conditioning chamber containing the same exact context but with no administration of a CS or foot shock. Freezing was analyzed for 1–3 min. One hour later, the mice were placed in a new context containing a different odor, cleaning solution, floor texture, chamber walls and shape. Animals were allowed to explore for 2 min before being re-exposed to the CS. Freezing was analyzed for 1–3 min. Freezing was measured using a FreezeScan video tracking system and software (Cleversys, Inc).

RAWM. Our paradigm followed a previously described protocol[35]. The goal arm location containing a platform remained constant throughout the training and testing phases, and the start arm was changed during each trial. On day 1 during the training phase, mice were trained for 15 trials, with trials alternating between a visible and a hidden platform. On day 2 during the testing phase, mice were tested for 15 trials with a hidden platform. Entry into an incorrect arm was scored as an error, and errors were averaged over the training blocks (three consecutive trials).

Plasma collection. Pooled mouse plasma was collected from 700 young (3 months) or aged (18 months) mice by intracardial bleed at time of euthanasia. Plasma was prepared from blood collected with EDTA followed by centrifugation at 1,000*g*. For plasma denaturation, plasma was heated for 2–3 min at 95 °C, followed by a short spin at 1,000*g*. All plasma aliquots were stored at −80 °C until use. Before administration, plasma was dialyzed using 3.5-kDa D-tube dialyzers (EMD Millipore) in PBS to remove EDTA. Young adult mice were systemically treated with plasma (100 µl per injection) isolated from young or aged mice by intraorbital injections or intravenously into the tail vein eight times over 24 d.

Corticosterone analysis. Blood was obtained from each mouse in a pair by serial submandibular bleeding under rapid isoflurane exposure; the sampling site on the muzzle was alternated for each time point to minimize discomfort. Plasma was isolated and stored at −80 °C until measurement of the stress-response hormone corticosterone (CORT) by a competitive CORT ELISA (Enzo Life Sciences). Urine was obtained by placing each pair on a wire-cage hopper and palpating the bladder to void urine into individual Eppendorf tubes for each mouse of the pair. Samples for all time points were collected according to a strict schedule to minimize circadian fluctuations in blood hormone concentrations. Urine CORT was measured according to manufacturer recommendations using the CORT ELISA kit (Enzo Life Sciences). Raw absorbance values for all CORT ELISAs were obtained from a microtiter plate reader at an absorbance of 405 nm. CORT concentrations of test samples were calculated from a four-parameter logistic curve fit of the percentage steroid bound versus the [CORT] of the standards.

Data and statistical analyses. All experiments were randomized and performed by a blinded independent researcher. Researchers remained blinded throughout histological, biochemical and behavioral assessments. Groups were unblinded at the end of each experiment before statistical analysis. Data are expressed as the mean ± s.e.m. The distribution of the data in each set of experiments was tested for normality using the D'Agostino-Pearson omnibus test or the Shapiro-Wilk test. No significant differences in variance between groups were detected using an *F* test. Statistical analyses were performed with Prism 5.0 software (GraphPad Software). Means between two groups were compared with a two-tailed, unpaired Student's *t* test. Comparisons of means from multiple groups with each other or against one control group were analyzed with one-way ANOVA followed by the appropriate *post-hoc* tests (as indicated in the figure legends). All histology, electrophysiology and behavior experiments were conducted in a randomized and blinded fashion.

28. Smolinsky, A.N. *et al*. Analysis of grooming behavior and its utility in studying animal stress, anxiety, and depression. in *Mouse Models of Mood and Anxiety Disorders* (ed. Gould, T.) 21–36 (Humana Press, NY, 2009).
29. Gould, T.D. *Mood and Anxiety Related Phenotypes in Mice: Characterization Using Behavioral Tests* (Humana Press, New York, 2009).
30. Luo, J. *et al*. Glia-dependent TGF-β signaling, acting independently of the TH17 pathway, is critical for initiation of murine autoimmune encephalomyelitis. *J. Clin. Invest.* **117**, 3306–3315 (2007).
31. Xie, X. & Smart, T.G. Modulation of long-term potentiation in rat hippocampal pyramidal neurons by zinc. *Pflugers Arch.* **427**, 481–486 (1994).
32. Grimm, D. *et al*. *In vitro* and *in vivo* gene therapy vector evolution via multispecies interbreeding and retargeting of adeno-associated viruses. *J. Virol.* **82**, 5887–5911 (2008).
33. Xu, W. *et al*. Distinct neuronal coding schemes in memory revealed by selective erasure of fast synchronous synaptic transmission. *Neuron* **73**, 990–1001 (2012).
34. Raber, J. *et al*. Irradiation enhances hippocampus-dependent cognition in mice deficient in extracellular superoxide dismutase. *Hippocampus* **21**, 72–80 (2011).
35. Alamed, J., Wilcock, D.M., Diamond, D.M., Gordon, M.N. & Morgan, D. Two-day radial-arm water maze learning and memory task; robust resolution of amyloid-related memory deficits in transgenic mice. *Nat. Protoc.* **1**, 1671–1679 (2006).

doi:10.1038/nm.3569